Analytical Biochemistry 465 (2014) 156–163

Contents lists available at ScienceDirect

Analytical Biochemistry

journal homepage: www.elsevier.com/locate/yabio

Localized surface plasmon resonance-based DNA detection in solution using gold-decorated superparamagnetic Fe_3O_4 nanocomposite

Arghya Bandyopadhyay, Keka Sarkar *

Department of Microbiology, University of Kalyani, Kalyani, Nadia, West Bengal 741235, India

ARTICLE INFO

Article history:
Received 19 March 2014
Received in revised form 8 July 2014
Accepted 24 July 2014
Available online 1 August 2014

Keywords:
Magneto–optical nanocomposite
Gold nanoparticle
Sensors
SPR

ABSTRACT

In the field of nucleic acid-based biosensor technology, DNA-conjugated nanocomposites have attracted much attention due to their unique properties and multimodal applicability. However, quantitative estimation of sequence-specific oligonucleotide in a simpler way is still a challenge. Precise positioning of DNA probes over the surface of the nanocomposite can overcome problems such as steric hindrance of the surface-bound molecules to enable further sensing as well as nonspecific folding of the DNA molecule over the surface of the gold (Au) nanolayer. Considering such objectives, we have developed glutathionated Fe_3O_4@Au core/shell nanocomposite, fabricated with DNA molecules and applied for sensing complementary oligo spectrophotometrically, using the localized surface plasmon resonance (LSPR) properties of the synthesized nanocomposite. When hybridization experiments were performed with 10 to 100 fM complementary DNA and DNA-conjugated nanocomposite, a strong linear relationship was observed between DNA concentration and surface plasmon resonance (SPR). Discrimination even at the single-base level was also observed when further experiments were performed with complementary DNA, but with a sequential decrease of bases from the single level to the fifth level.

Development of highly sensitive biosensors composed of miniaturized signal transducer elements that can enable the real-time parallel monitoring of multiple species for the diagnosis and detection of diseases, drug discovery, and environmental detection of biological agents imposes stringent requirements [1,2]. Much biosensor research has been devoted to the evaluation of various signal transduction systems, and optical sensors based on surface plasmon polaritions using gold nanoparticles for bioanalysis are becoming a preferred method for many sensing applications [3–15]. Plasmon resonances impart noble metal nanoparticles with unusual optical properties that have been employed in a wide range of applications, including imaging and chemical and biological sensing and probing, delivering remarkable sensitivity. On the other hand, superparamagnetic iron oxide nanoparticles (SPIONs)[1] consisting of maghemite (γ-Fe_2O_3) or magnetite (Fe_3O_4) have attracted much interest due to their potential applications in magnetically guided drug delivery [16], specific targeting and imaging of cancer cells [17], hyperthermia treatment of solid tumors [18], and contrast enhancement agents in magnetic resonance imaging [19]. However, the extent of biomedical applications of SPIONs strongly depends on their stability in physiological solutions and the extent to which their surfaces can be chemically functionalized. Coating SPIONs with an organic shell, such as macrocyclic surfactants [20] or polymers [21], or an inorganic shell [22] can enhance their stability, dispersibility, and functionality of the otherwise naked magnetic nanoparticles. Although coating of magnetic nanoparticles with polymers and silica shells has been studied extensively, there are limited reports on the coating of SPIONs with organically active metallic shells.

For biomedical applications, elemental gold is an ideal coating due to its low reactivity, high chemical stability, and biocompatibility as well as its affinity for binding to amine (-NH_2) or thiol (-SH) terminal groups of organic molecules [3]. Moreover, the gold shell furnishes SPIONs with plasmonic properties [23], thereby imparting a 6-fold enhancement in trapping efficiency and detection sensitivity as compared with similar-sized polystyrene particles. In addition, the absorption of irradiation by gold at the most common trapping wavelength (1064 nm) imparts a dramatic heating of the particles (266 °C/W) [24], with Au-coated SPIONs serving as an excellent heating source following magnetic targeting of a tumor [25,26].

The synthesis of Fe_3O_4@Au core–shell nanoparticles is challenging because the surface energies of the two materials are different

* Corresponding author.
E-mail address: drkekasarkar@yahoo.com (K. Sarkar).

[1] *Abbreviations used:* SPION, superparamagnetic iron oxide nanoparticle; Fe_3O_4, magnetite; SPR, surface plasmon resonance; TEM, transmission electron microscopy; EDAX, energy-dispersive X-ray analysis spectroscopy; AFM, atomic force microscopy; XRD, X-ray diffraction; UV–vis, ultraviolet–visible; TCEP, tris(2-carboxyethyl) phosphine.

http://dx.doi.org/10.1016/j.ab.2014.07.025
0003-2697/

[27]. Consequently, gold nanoparticles tend to nucleate rapidly, forming discrete nanoparticles in solution without coating the surface of magnetite. Core–shell nanoparticles of Fe_3O_4 on gold ranging from 18 to 30 nm in size have also been prepared, using a reverse micelle method [28], but are capped with organic surfactants, rendering them unsuitable for biomedical applications as they disperse in organic solvents. Recently, hydrophobic Fe_3O_4 on gold core–shell nanoparticles were prepared by reducing $HAuCl_4$ in a chloroform solution of oleylamine as a surfactant, followed by transferring to the aqueous phase by mixing them with an aqueous cetyltrimethylammonium bromide (CTAB) [29]. Overall, it is evident that a simple aqueous-based synthetic method to coat Fe_3O_4 nanoparticles with uniform and relatively thin layers of a noble metal (Au) shell that causes minimal perturbations to the magnetic properties is an important objective for applications in the biomedical field.

Several attempts have been made to use colloidal gold nanoparticles for biodetection and used for various bioapplications [5,7,10,12], but among the available nanosensing techniques for molecular diagnostics, various complex systems such as solid support-based surface plasmon resonance (SPR), lab-on-chip-based substrates, and microarray-based detection (see S:6 in online supplementary material) are the most used. To increase the efficiency and sensitivity with minimal scientific overhead and cost for the detection of targeted DNA sequence, our study focused on two objectives. First, we developed a new strategy for the synthesis of SPR-based bimetallic superparamagnetic nanocomposite with an evenly fabricated predefined bioactive agent on the surface that is accessible for attachment of substrate without steric hindrance. Second, the nanocomposite was applied as a biosensor that can transduce the substrate–reactant reaction (DNA–DNA hybridization) response with measurable SPR peak shifting. Thus, both qualitative and quantitative evaluations of specific DNA sequence at the femtomole (fM) level can be done in a very rapid and reproducible way in solution.

Materials and methods

General information

Deionized nanopure water, filtered through a 0.015-μm membrane filter (Nuclepore, Whatman), was used throughout. All chemicals for the synthesis of nanoconjugate were purchased from Sigma–Aldrich and used without further purification. The oligos were purchased from BioServe Biotechnologies India (Hyderabad, India). The transmission electron microscopy (TEM) images were taken by using an FEI Tecnai S-twin transmission electron microscope at an accelerating voltage of 200 kV. The composition of Fe_3O_4@Au nanoparticles was characterized using a Hitachi S-3200 scanning electron microscope for energy-dispersive X-ray analysis spectroscopy (EDAX). Atomic force microscopy (AFM) analysis of Fe_3O_4@Au seeds and Fe_3O_4@Au nanocomposites was carried out in Veeco di CP-II atomic force microscope. X-ray diffraction (XRD) on dried nanoparticles was performed in a Siemens D500 X-ray diffractometer (Siemens, Berlin, Germany) within a 2θ range of 20 to 80 °C using CuKα radiation. Magnetic measurements were carried out on a SQUID magnetometer (MPMS, Quantam Design, USA). The ultraviolet–visible (UV–vis) absorption was measured with a Techcomp UV2300II UV–vis analytic spectrophotometer (Techcomp, China).

Synthesis of nanocomposite

Synthesis of glutathione-functionalized iron oxide nanoparticles

The 8-nm iron oxide nanoparticles (Fig. 1A) having a net negative interfacial charge at pH 7.0 were synthesized in aqueous medium following the basic chemical coprecipitation method described in our previous report [30]. Glutathione-modified magnetic particles were synthesized by mixing glutathione and Fe_3O_4 nanoparticles and sonicated for 1 h at room temperature under basic conditions (∼pH 9.0 ± 0.5).

Synthesis of glutathione-functionalized gold nanoseeds

Glutathione-modified gold seeds were prepared by the method described elsewhere [31]. Typically, 3.0 mM glutathione was dissolved in 40 ml of water, and 1.0 mM $HAuCl_4$ was dissolved in 80 ml of methanol. These two solutions were mixed under stirred conditions, resulting in a cloudy white suspension. After that, 10 ml of 10 mM $NaBH_4$ solution was added under high-speed stirring (∼1500 rpm with a mechanical stirrer [IKA 20]). The addition of $NaBH_4$ solution changed the color of the suspension to dark brown, indicating the formation of large glutathione MPC (monolayer protected cluster) compounds of gold. After an additional 1 h of stirring, the solution was washed thoroughly to remove unreacted chemicals and evaporated under a vacuum at 43 °C until dark slurry of the cluster compounds was formed.

Synthesis of glutathione–gold seed-functionalized iron oxide nanoparticles

For the preparation of gold-seeded magnetic nanocomposite, we followed the method of Chin and coworkers [32] with some modifications. Equal volumes of the glutathionated Au seed suspension and glutathione-coated Fe_3O_4 nanoparticles were taken, and the mixture was stirred overnight before being centrifuged and washed thoroughly to remove free Au seeds. The precipitate was redispersed in 50 ml of water and sonicated for 1 h prior to further modification.

Synthesis of glutathione-functionalized Fe_3O_4@Au core–shell nanocomposite

Here, 10 mM 5-ml aqueous solution of $HAuCl_4$ was added to the sonicated 50 ml of Au seed-decorated Fe_3O_4 nanoparticles under mixing. To assist the reaction, the pH of the mixture was adjusted to slightly basic (∼pH 9.0) by the addition of aqueous NH_3. Then 1.5 times excess saturated dextrose solution was added dropwise into the solution to reduce the $HAuCl_4$ onto the Au seed-decorated Fe_3O_4 nanoparticle surface.

Preparation of DNA-functionalized Fe_3O_4@Au core–shell nanocomposite

Then, 5′ thiol-modified oligonucleotides were attached to the prepared nanocomposite following the method described by Ackerson and coworkers [33]. Here, 23 residue oligonucleotides (thiol 5′-ACCGCCCGTCACACCATGGGAGT-3′ was used as the main probe, and the oligo having the sequence 5′-ACTCCCATGGTGTGACGGG CGGT-3′ was used as the complementary DNA strand) were reduced with the aid of tris(2-carboxyethyl)phosphine (TCEP). The reaction was conducted using the following ratio of thiol-modified oligo: TCEP (10:1 μl, v/v) and 500 μM:50 mM of strength. The 5′-thiol modified oligo was kept with TCEP for 30 min at room temperature. Finally, the nanocomposite (10 μl of the solution having 0.05 OD value at 531 nm) was added, followed by incubation for 1 h at 50 °C.

Oligo probe hybridization assay

Oligo hybridization reactions were carried out after dispersion of oligo probe nanocomposite in hybridization reaction buffer (10 mM Tris base and 1.5 mM $MgCl_2$, pH 8.0). For the hybridization, 25 μl of DNA-functionalized nanocomposite was mixed with 10 μl of 50 pM complementary and semi-complementary probes separately in different tubes, and then the tubes were placed in a

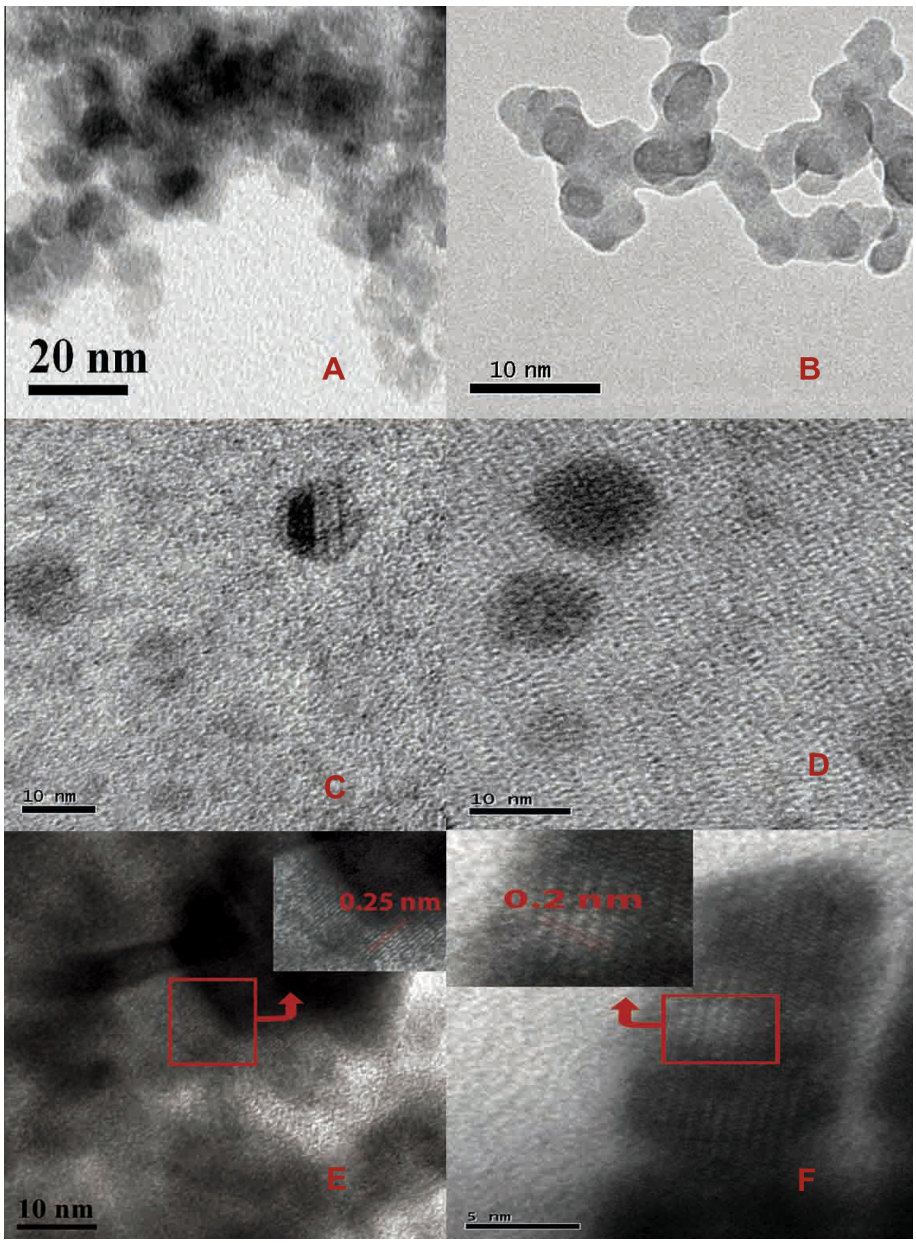

Fig.1. TEM images of synthesized nanoparticles and nanocomposites. (A) Iron oxide nanoparticle. (B) Glutathione-modified gold nanoparticle. (C) Glutathione-modified gold-seeded iron oxide nanocomposite: A single nanocomposite showing the partial seeding of iron oxide nanoparticle. The dark contrasting parts are the gold seeds. (D) Fully synthesized final core–shell nanoparticle. High-resolution TEM images of panels A and B are represented in panels E and F, respectively, along with lattice patterns shown in the insets.

thermal cycler under the following conditions: denaturation for 5 min at 95 °C and hybridization for 3 min at 45 °C. The unbound probes are separated by magnetic separation on a magnetic rack for 5 min. The pellet of the composite was redispersed in 3 ml of water for further UV–vis spectral analysis. Details of all the probes used are given in S:5 of the supplementary material.

Results and discussion

Here, we report a novel three-step synthetic approach to coat SPIONs with homogeneous gold shells with a specific number of glutathione islands/patches protruding from them. This straightforward approach affords core–shell nanoparticles with superparamagnetic properties while at the same time endowing the nanoparticles with plasmonic properties. Moreover the glutathionated portions are specifically accessible for binding of biological molecules (e.g., DNA oligos). Thus, this nanocomposite formulation delivers unique appearance, processing, and performance characteristics.

The overall synthetic process of the oligo surface-active Fe_3O_4@gold core–shell nanoparticles was performed by the following steps (Scheme 1): (i) synthesis of glutathione-functionalized 8-nm Fe_3O_4 nanoparticles; (ii) these were first coated with 2 nm glutathione-modified gold seeds; (iii) a further coating experiment was carried out by gently reducing $HAuCl_4$ in a dextrose solution in the presence of (ii); the prepared core–shell nanocomposites were water soluble and well stabilized; (iv) 5′ thiol-modified oligonucleotides were attached to the nanocomposite (iii) by thiol bonding.

Characterization of synthesized nanoparticles and nanocomposite

TEM analysis (Fig. 1A and D) revealed that the overall diameter of Fe_3O_4@Au nanoparticles increased from 8 nm to approximately 11 nm. The monodispersity and surface charge of the synthesized

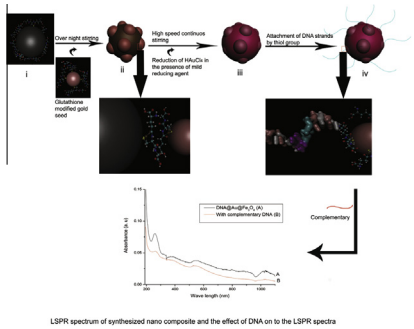

Scheme 1. Scheme for DNA-conjugated nanocomposite synthesis.

particles were analyzed and are presented in S:1 of the supplementary material. The presence of glutathione on the surface of the nanocomposite was confirmed using EDAX and is evidenced by the peak characteristics (see S:2 in supplementary material). The composition of the nanoparticles was estimated from the presence of carbon, hydrogen, nitrogen, oxygen, sulfur, iron, and gold. The EDAX results indicated that the molar ratio between Fe and Au was 16.82:1.85. Absence of a distinctive shell and inner iron oxide core in the composite (Fig. 1F) was observed as the core was masked due to the presence of a higher electron density of Au outside the construction. Fig. 1C represents partially gold-seeded iron oxide nanoparticles, to evidence the construction, and lower electron dense iron oxide was imperceptible behind the higher electron dense Au, as already discussed above (shown in Fig. 1F). In Fig. 1C, the dark parts are the Au seeds, whereas the lighter parts are the core material (i.e., iron oxide). Thus, prolonged exposure of glutathione-modified gold seed and glutathione-modified iron oxide under high-speed stirring conditions, as reported previously by Chin and coworkers [32], can generate a composite of these two nanostructures.

The lattice fringes of the shell clearly indicate (inset of Fig. 1F) the spacing of approximately 2.0 Å lattice planes for gold, whereas high-resolution TEM images of core particles show crystal lattices that represent the iron core with interplanar distances of approximately 2.5 Å. The inset of Fig. 1E indicates that the interplane interval of Fe_3O_4 nanoparticles was approximately 2.5 Å, with (311) facet of face-centered cubic Fe_3O_4 crystals. In addition, the interplane interval of approximately 2.0 Å in the inset of Fig. 1F is consistent with that of (111) facet of a face-centered cubic Au crystal. Overall, these results illustrate that the resultant Fe_3O_4–Au coats were Fe_3O_4/Au core–shell nanocomposites.

The morphology and surface of synthesized nanocomposite were further studied by AFM. Because the surface morphology of the pre-final or gold-seeded Fe_3O_4 nanocomposite is a crucial factor for the construction of final nanocomposite, only these two stages of the synthesis phase were characterized using AFM. It was expected that the gold seeds over the surface of the core material would be visible by this technique. The roughness of the composite should be higher in the case of the pre-final particle than in the case of the final particle itself because the final particle was further coated with a very fine homogeneous Au shell. The atomic force micrograph of pre-final composite is presented in Fig. 2A, and the surface morphology of the final synthesized nanocomposite is shown in Fig. 2B. S:3 in the supplementary material summarizes the key AFM features obtained in the case of both pre-final and final nanocomposites. Thus, from AFM analysis, we observe that the nanocomposite shows the characteristics as expected.

To achieve the predefined positioning of the biomolecule of interest over the surface of the nanocomposite, we envisioned a structure resembling an "acupuncture ball" in which the pre-active spikes are the only places where the biomolecules will be attached. From the analysis of surface of the final nanocomposite, it is clear that the "glutathione-activated golden spikes" are present on the surface for further reaction. In contrast, the valleys offer no activity for further modification after the final gold shell deposition.

XRD patterns for Fe_3O_4 (Fig. 3A), Au (Fig. 3B), Au-seeded Fe_3O_4 (Fig. 3C), and Fe_3O_4@Au (Fig. 3D) core–shell nanoparticles demonstrate characteristic peaks. The diffraction peaks at 2θ (30.0°, 35.3°, 43.0°, 56.9°, and 62.5°) corresponding to (220), (311), (400), (511), and (440) indicate that the nanoparticles were pure Fe_3O_4 crystal in the curve in Fig. 3A. The curve in Fig. 3B has diffraction peaks at 2θ (38.2°, 44.4°, 64.6°, and 77.5°) that can be assigned to (111), (200), (220), and (311) planes for gold in the cubic phase. The peaks of the curve in Fig. 3C represent both iron oxide nanoparticles and gold nanoparticles. The XRD spectrum of the final Fe_3O_4@Au nanoparticles (the curve in Fig. 3D) has sharp peaks, consistent with an Au nanocrystal, and an absence of peaks observed for Fe_3O_4 nanoparticles in the curves in Fig. 3A and C, indicating complete coverage by Au (i.e., a core–shell structure). This further confirms that the iron oxide nanoparticles can be successfully coated and passivated by the gold shell, as reported previously [29,34].

The Fe_3O_4@Au core–shell nanoparticles were superparamagnetic at room temperature given that the magnetization measurement

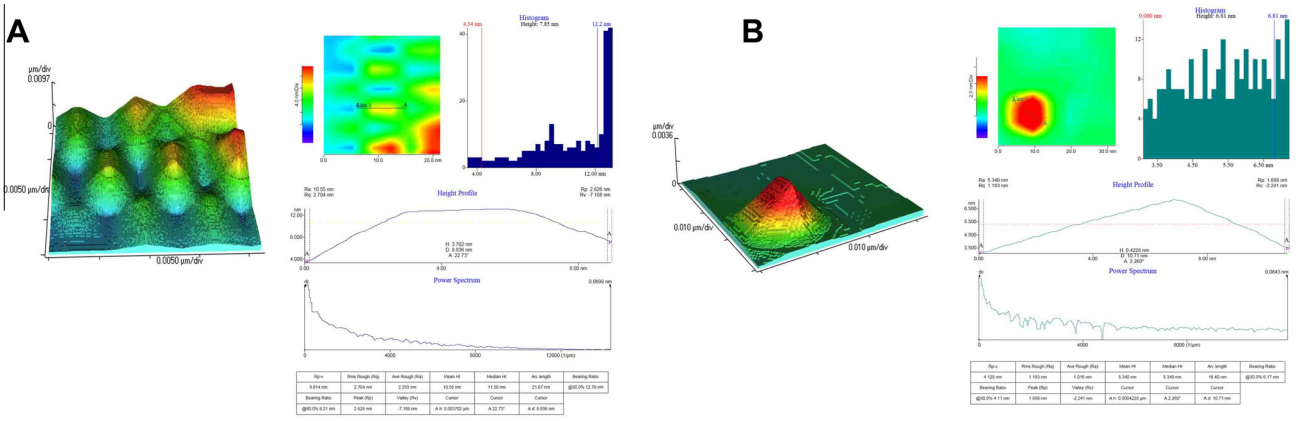

Fig.2. AFM images of pre-final and finally synthesized nanocomposite. (A) AFM image of pre-final nanocomposite: Line analysis showing the surface features of the synthesized composite. (B) AFM image of a single final nanocomposite: Line analysis showing the surface features of the synthesized composite.

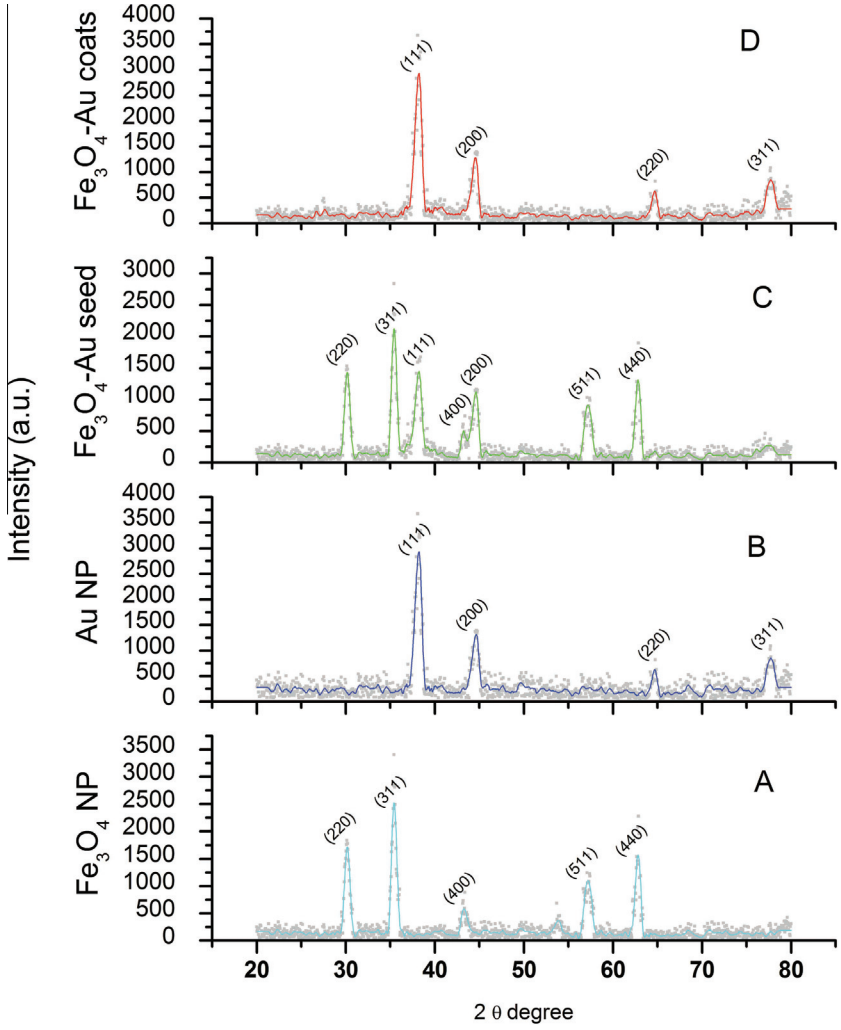

Fig.3. XRD patterns of synthesized nanoparticles and nanocomposite—Fe_3O_4 (A), Au (B), Au-seeded Fe_3O_4 (C), and Fe_3O_4@Au (D)—shown with their respective indexes. All data shown are 51 point Savitzky–Golay smoothed curves. NP, nanoparticles.

shows a typical superparamagnetic S-like curve. Fig. 4 shows the hysteresis loop (magnetization [M] vs. applied field [H], i.e., an M–H curve) measured at 300 and 4 K. The core–shell particles exhibited an intrinsic coercivity (H_{ci}, marked at the intercept of the curve and the negative H axis) of 33.98 Oe at 300 K and 358.84 Oe at 4 K (shown in inset of Fig. 4A). Although an intrinsic coercivity of 31.58 Oe at 300 K and of 356.44 Oe at 4 K (shown in inset of Fig. 4B) was revealed by the iron oxide nanoparticles. The magnetic remanence (M_r is the remanent magnetization at $H = 0$, marked at the intercept of the curve and the positive M axis) is 0.048 emu/g at 4 K and 0.005 emu/g at 300 K for the core iron oxide nanoparticles, and the value remained almost unchanged (i.e., 0.042 emu/g at 4 K and 0.006 emu/g at 300 K) after gold coating (shown in insets of Fig. 4).

UV–vis absorption spectral band patterns (see S:4 in supplementary material) were analyzed for major products at each step of the nanocomposite synthesis. In S:4, curves A and B represent band patterns of core iron oxide nanoparticles and glutathione-modified iron oxide nanoparticles, respectively, and do not show any measurable features in the visible region despite some differences. The change in band patterns is presumably associated with the modifications. However, curve E illustrates the band of the final Au-coated nanoparticle with a peak at 531 nm, which is not observed in glutathionated Au (curve C) or Au-seeded iron oxide nanoparticles (curve D). Glutathionated gold seeds (curve C) displayed a characteristic SPR peak at 525 nm, whereas Au-seeded nanocomposite (curve D) exhibited the SPR peak at 508 nm.

The synthetic approach for the nanocomposite uses glutathione as an anchoring molecule for the glutathione-modified gold seeds. Here, glutathione-modified iron oxide nanoparticles electrostatically interact with glutathione-modified gold seeds (a prolonged exposure for overnight stirring facilitates this interaction; the detailed method is given below). The gold seeds act as crystallization nucleation sites on which a continuous gold shell can be formed on $HAuCl_4$ reduction, leaving the glutathionated portions of the gold seeds as an island for the further reaction(s).

The sequential attachment of DNA probe on the gold surface of the nanocomposite resulted in red shifting of the plasmon resonance spectra (Fig. 5A). According to the previous report of Ackerson and coworkers [33], the presence of glutathione over the surface of gold nanolayer facilitates a place exchange reaction, known as a Murray place exchange reaction [35], between glutathione and thiol-modified DNA. Hence, the attachment of thiolated DNA arises only on exposed Au seed regions because these were the only glutathionated areas on the finally synthesized particles.

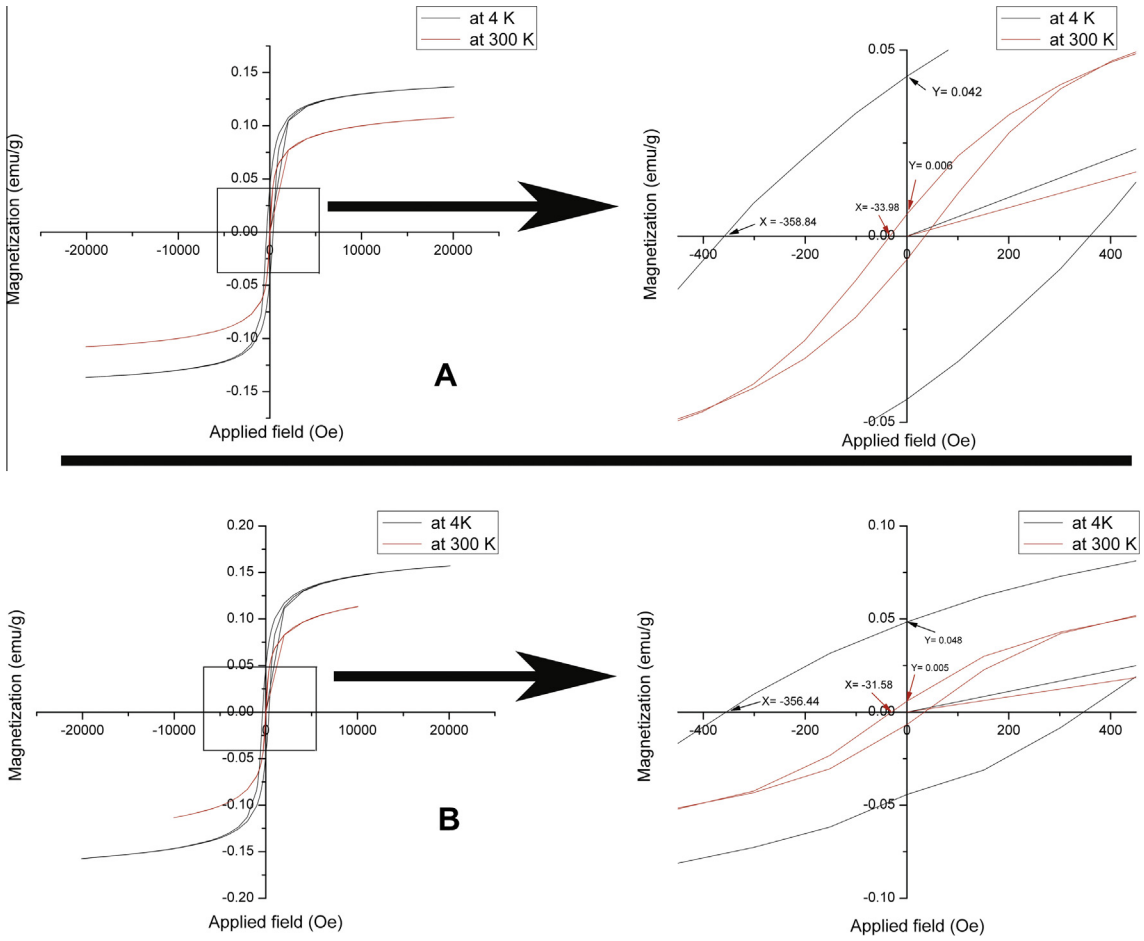

Fig.4. Hysteresis loop of Fe_3O_4@Au core–shell nanoparticle (A) and Fe_3O_4 nanoparticle (B). Magnified regions of each loop show the detailed values of *M–H* hysteresis curve.

Furthermore, we extended our experiment using this engineered nanoparticle for biological sensing via complementary DNA probes.

SPR-based biomolecular recognition using the synthesized nanocomposite

We have already seen that, due to thiol-specific attachment of DNA on the synthesized nanocomposite, the SPR peak was found at 545 nm (shown in Fig. 5A). When the DNA-probed nanocomposite was incubated with complementary DNA in spiked sample, the SPR peak shifted to 535 nm. On the contrary, in the presence of less than 50% complementary DNA, the SPR peak was found to be at 541 nm (Fig. 5B). The blue shifting of the SPR peak indicated the disaggregation of the nanocomposite in the presence of paired DNA strands. The disaggregation of the nanocomposite increased with increasing degrees of complementarity of the DNA.

The changes in the optical properties of the oligonucleotide-coated colloidal gold in the presence of complementary oligonucleotide can be explained by the previous report of Lazarides and Schatz [36], who pointed out that the aggregation-induced shifting and broadening of the plasmon peak is a manifestation of the development of a collective response involving the electrons of networked particles that assemble in regions with dimensions on the order of visible wavelength.

Fig. 5D shows the changes in SPR peak intensities with different concentrations of complementary DNA strands. To quantify complementary DNA, a graphical representation was plotted in order to relate the concentration of complementary DNA with the vertical shifting of SPR peak at 534 nm. It was observed that, along with increasing concentrations of input of complementary DNA, the values of wavelengths went down gradually (Fig. 5D). The statistical coefficient R^2 is 0.997 (inset of Fig. 5D), suggesting good linearity that demonstrates the possibility of using our method to accurately detect the minimum concentration of specific targeted DNA in sample. Fig. 5D revealed that Fe_3O_4@Au nanocomposite could efficiently detect the full complementary DNA (23 bp) at a 10-fM concentration.

Furthermore, to explore the sensitivity of single-base change in the length of the complementary DNA, we repeated our experiments using complementary DNA with base shortening at the 5′ end with increasing orders up to five bases. The SPR peak shifting was still observed (Fig. 5C), whereas the linearity still held. The linear statistical coefficient (R^2 = 0.989) revealed the authenticity of the proposed method (inset of Fig. 5C).

Hence, our method was proved to be effective, simple, and easy to perform, and it could be used to conduct the detection of biomarkers related to various diseases. As a promising technology, sequence-specific DNA detection by the aid of nanotechnology has been widely used. However, quantitative detection of complementary DNA at the fM level in a simpler way is still a challenge. In this study, we performed a quantitative exploration of the relationship between complementary DNA concentration and detection limit up to single-base shortening in complementary sequences and SPR peak shifting.

Compared with frequently used methods, such as fluorescent, radiolabeled, solid support-based SPR and high-throughput microarray (see S:6 in supplementary material), our solution mode

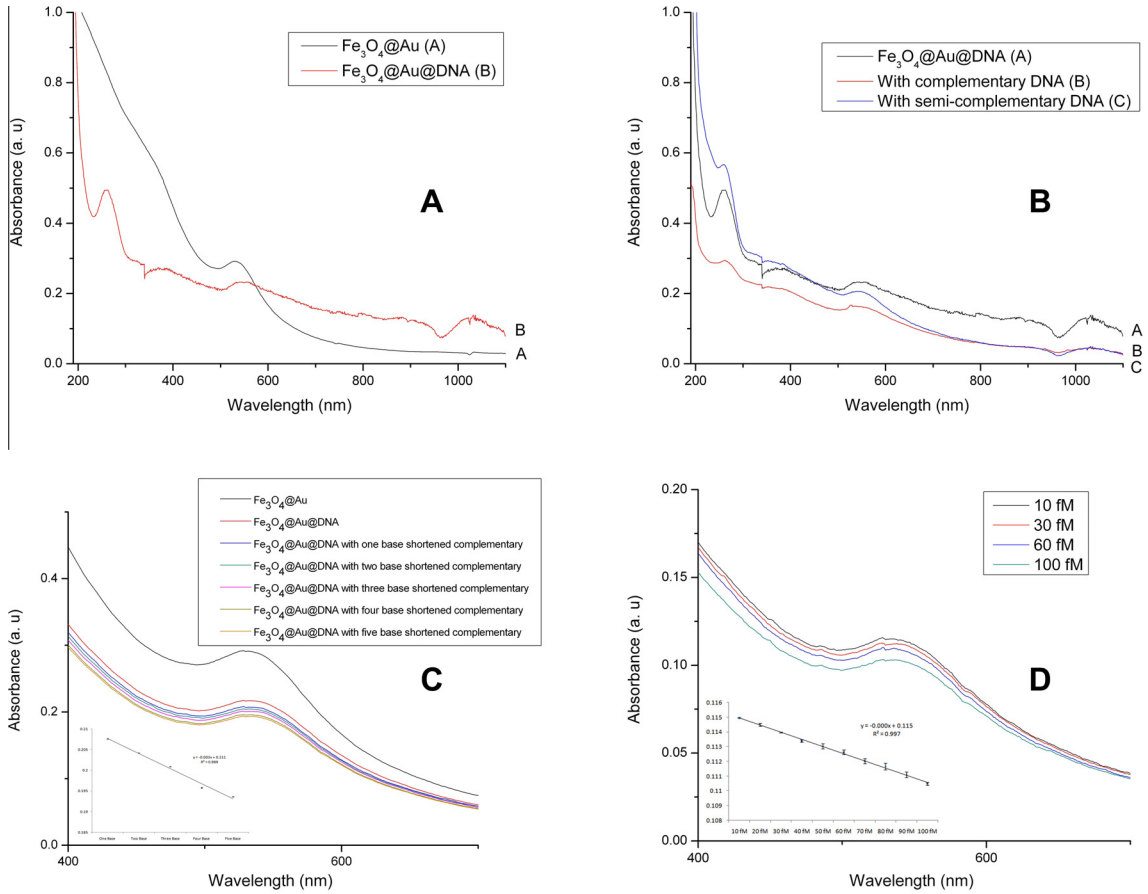

Fig.5. Changes observed in SPR peak of finally synthesized nanocomposite due to the presence of different types and concentration of oligos. (A) SPR spectrum of final nanocomposite and the DNA-probed final composite showing the discriminating SPR spectral feature. (B) Detection and discrimination of complementary and semi-complementary DNA oligos by SPR peak character change. The UV–vis absorbance of oligo-probed final nanocomposite is shown in curve A, and the UV–vis absorbance after the addition of complementary oligo is shown in curve B. Curve C represents the presence of semi-complementary oligo. (C) Effect of the presence of length-shortened complementary oligos on the DNA-probed nanocomposite. (D) Detection limit of synthesized oligo-probed nanocomposite testing using different concentrations of complementary oligo. Insets of panels C and D represent regression analysis of corresponding experiments. In the case of the inset of panel D, the regression analysis was done from 10 to 100 fM, but for better data representation the graph is plotted for the indicated four concentrations. All of the data for both experiments were performed in triplicates, and regression analysis was done on obtained data.

nanocomposite/SPR-based technique has the following unique advantages. Our method is simple and quick, taking a maximum of 20 min for detection, whereas the above-mentioned commonly used techniques require several relatively complicated and time-consuming steps to obtain desirable results. Microarray, considered a relatively easy and quick approach, still requires a whole set of micro machine devices to anchor oligonucleotides onto substrates and is more costly than our method.

Microarray required highly purified samples, and results are sensitive to contamination. Our method, on the other hand, only required DNA contaminated sample because the presence of core material in the nanocomposite can preconcentrate bound DNA in the presence of magnet before SPR measurements.

Conclusions

Glutathionated Fe_3O_4@Au core–shell nanocomposite covered with oligo DNA molecules was synthesized and applied for sensing complementary oligo DNA spectrophotometrically using the localized SPR properties of the synthesized nanocomposite. The analytical performance of the synthesized nanocomposite was evaluated using complementary oligonucleotide targets without prelabeling, making the protocol simple and reproducible and offering higher sensitivity. However, the presence of the magnetic core facilitated easy separation of the attached DNA target from the sample using a magnet and washing. This simple spectrophotometric method may provide a viable alternative to other sensitive electrochemical, fluorescence, and radioactively labeled DNA assays.

In the future, precise quantification of DNA hybridization in a solution format may be accomplished by further calibration of the number of attached DNA molecules. Furthermore, this approach could be applied to construct a multimodal detection sensor by attaching a number of different compatible biomolecules to the bioactive surface. Thus, this new strategy for synthesis of SPR-based nanosensors is a promising route for the construction of assays for biomedical and other applications.

Acknowledgments

This work was jointly supported by funding from the Department of Science and Technology, Government of India (Project Nanomission, SR/NM/NS-48/2009), and the DST–PURSE Programme, University of Kalyani, Nadia, West Bengal. A.B. is personally grateful for the scholarship support from the University of Kalyani. We are also thankful to the Biophysics Division of the Saha Institute of Nuclear Physics (SINP, Kolkata, India) for the electron microscope facility and to the Indian Association for the Cultiva-

tion of Science (IACS, Kolkata) for XRD, SQUID, SEM, and AFM facilities.

Appendix A. Supplementary data

Supplementary data associated with this article can be found, in the online version, at http://dx.doi.org/10.1016/j.ab.2014.07.025.

References

[1] A.P.F. Turner, Biosensors—sense and sensitivity, Science 290 (2000) 1315–1317.
[2] A.J. Haes, R.P. Van Duyne, A nanoscale optical biosensor: sensitivity and selectivity of an approach based on the localized surface plasmon resonance spectroscopy of triangular silver nanoparticles, J. Am. Chem. Soc. 124 (2002) 10596–10604.
[3] M.-C. Daniel, D. Astruc, Gold nanoparticles: assembly, supramolecular chemistry, quantum-size-related properties, and applications toward biology, catalysis, and nanotechnology, Chem. Rev. 104 (2004) 293–346.
[4] R. Elghanian, J.J. Storhoff, R.C. Mucic, R.L. Letsinger, C.A. Mirkin, Selective colorimetric detection of polynucleotides based on the distance-dependent optical properties of gold nanoparticles, Science 277 (1997) 1078–1081.
[5] L. He, M.D. Musick, S.R. Nicewarner, F.G. Salinas, S.J. Benkovic, M.J. Natan, C.D. Keating, Colloidal Au-enhanced surface plasmon resonance for ultrasensitive detection of DNA hybridization, J. Am. Chem. Soc. 122 (2000) 9071–9077.
[6] J.C. Love, L.A. Estroff, J.K. Kriebel, R.G. Nuzzo, G.M. Whitesides, Self-assembled monolayers of thiolates on metals as a form of nanotechnology, Chem. Rev. 105 (2005) 1103–1170.
[7] S. Mann, W. Shenton, M. Li, S. Connolly, D. Fitzmaurice, Biologically programmed nanoparticle assembly, Adv. Mater. 12 (2000) 147–150.
[8] B.R. Martin, D.J. Dermody, B.D. Reiss, M. Fang, L.A. Lyon, M.J. Natan, T.E. Mallouk, Orthogonal self-assembly on colloidal gold–platinum nanorods, Adv. Mater. 11 (1999) 1021–1025.
[9] C.A. Mirkin, R.L. Letsinger, R.C. Mucic, J.J. Storhoff, A DNA-based method for rationally assembling nanoparticles into macroscopic materials, Nature 382 (1996) 607–609.
[10] J.-M. Nam, C.S. Thaxton, C.A. Mirkin, Nanoparticle-based bio-bar codes for the ultrasensitive detection of proteins, Science 301 (2003) 1884–1886.
[11] C.M. Niemeyer, Functional hybrid devices of proteins and inorganic nanoparticles, Angew. Chem. Int. Ed. 42 (2003) 5796–5800.
[12] N.L. Rosi, C.A. Mirkin, Nanostructures in biodiagnostics, Chem. Rev. 105 (2005) 1547–1562.
[13] T.A. Taton, C.A. Mirkin, R.L. Letsinger, Scanometric DNA array detection with nanoparticle probes, Science 289 (2000) 1757–1760.
[14] A.G. Tkachenko, H. Xie, D. Coleman, W. Glomm, J. Ryan, M.F. Anderson, S. Franzen, D.L. Feldheim, Multifunctional gold nanoparticle–peptide complexes for nuclear targeting, J. Am. Chem. Soc. 125 (2003) 4700–4701.
[15] R. Wang, S. Tombelli, M. Minunni, M.M. Spiriti, M. Mascini, Immobilisation of DNA probes for the development of SPR-based sensing, Biosens. Bioelectron. 20 (2004) 967–974.
[16] J. Kim, J.E. Lee, S.H. Lee, J.H. Yu, J.H. Lee, T.G. Park, T. Hyeon, Designed fabrication of a multifunctional polymer nanomedical platform for simultaneous cancer-targeted imaging and magnetically guided drug delivery, Adv. Mater. 20 (2008) 478–483.
[17] S.T. Selvan, P.K. Patra, C.Y. Ang, J.Y. Ying, Synthesis of silica-coated semiconductor and magnetic quantum dots and their use in the imaging of live cells, Angew. Chem. Int. Ed. 46 (2007) 2448–2452.
[18] S.H. Wang, X. Shi, M. Van Antwerp, Z. Cao, S.D. Swanson, X. Bi, J.R. Baker, Dendrimer-functionalized iron oxide nanoparticles for specific targeting and imaging of cancer cells, Adv. Funct. Mater. 17 (2007) 3043–3050.
[19] Q.A. Pankhurst, J. Connolly, S. Jones, J. Dobson, Applications of magnetic nanoparticles in biomedicine, J. Phys. D 36 (2003) R167–R181.
[20] S.F. Chin, M. Makha, C.L. Raston, M. Saunders, Magnetite ferrofluids stabilized by sulfonato-calixarenes, Chem. Commun. (2007) 1948–1950.
[21] N. Shamim, L. Hong, K. Hidajat, M. Uddin, Thermosensitive polymer (*N*-isopropylacrylamide) coated nanomagnetic particles: preparation and characterization, Colloids Surf. B 55 (2007) 51–58.
[22] J. Choi, J.C. Kim, Y.B. Lee, I.S. Kim, Y.K. Park, N.H. Hur, Fabrication of silica-coated magnetic nanoparticles with highly photoluminescent lanthanide probes, Chem. Commun. (2007) 1644–1646.
[23] T.K. Sarma, A. Chattopadhyay, Starch-mediated shape-selective synthesis of Au nanoparticles with tunable longitudinal plasmon resonance, Langmuir 20 (2004) 3520–3524.
[24] Y. Seol, A.E. Carpenter, T.T. Perkins, Gold nanoparticles: enhanced optical trapping and sensitivity coupled with significant heating, Opt. Lett. 31 (2006) 2429–2431.
[25] X. Huang, P.K. Jain, I.H. El-Sayed, M.A. El-Sayed, Gold nanoparticles: interesting optical properties and recent applications in cancer diagnostics and therapy, Nanomedicine 2 (2007) 681–693.
[26] L. Hirsch, J. Jackson, A. Lee, N. Halas, J. West, A whole blood immunoassay using gold nanoshells, Anal. Chem. 75 (2003) 2377–2381.
[27] J. Lim, A. Eggeman, F. Lanni, R.D. Tilton, S.A. Majetich, Synthesis and single-particle optical detection of low-polydispersity plasmonic–superparamagnetic nanoparticles, Adv. Mater. 20 (2008) 1721–1726.
[28] M. Mandal, S. Kundu, S.K. Ghosh, S. Panigrahi, T.K. Sau, S. Yusuf, T. Pal, Magnetite nanoparticles with tunable gold or silver shell, J. Colloid Interface Sci. 286 (2005) 187–194.
[29] Z. Xu, Y. Hou, S. Sun, Magnetic core/shell Fe_3O_4/Au and Fe_3O_4/Au/Ag nanoparticles with tunable plasmonic properties, J. Am. Chem. Soc. 129 (2007) 8698–8699.
[30] A. Bandyopadhyay, S. Chatterjee, K. Sarkar, Rapid isolation of genomic DNA from *E. coli* XL1 Blue strain approaching bare magnetic nanoparticles, Curr. Sci. 101 (2011) 210–214.
[31] T.G. Schaaff, R.L. Whetten, Giant gold–glutathione cluster compounds: intense optical activity in metal-based transitions, J. Phys. Chem. B 104 (2000) 2630–2641.
[32] S.F. Chin, K.S. Iyer, C.L. Raston, Facile and green approach to fabricate gold and silver coated superparamagnetic nanoparticles, Cryst. Growth Des. 9 (2009) 2685–2689.
[33] C.J. Ackerson, M.T. Sykes, R.D. Kornberg, Defined DNA/nanoparticle conjugates, Proc. Natl. Acad. Sci. U.S.A. 102 (2005) 13383–13385.
[34] L. Wang, L. Wang, J. Luo, Q. Fan, M. Suzuki, I.S. Suzuki, M.H. Engelhard, Y. Lin, N. Kim, J.Q. Wang, Monodispersed core–shell Fe_3O_4@Au nanoparticles, J. Phys. Chem. B 109 (2005) 21593–21601.
[35] J.H. Michael, C.T. Allen, W.M. Royce, Dynamics of place–exchange reactions on monolayer-protected gold cluster molecules, Langmuir 15 (1999) 3782–3789.
[36] A.A. Lazarides, G.C. Schatz, DNA-linked metal nanosphere materials: structural basis for the optical properties, J. Phys. Chem. B 104 (2000) 460–467.